IOP Publishing Journal of Physics: Condensed Matter

J. Phys.: Condens. Matter **21** (2009) 115402 (7pp) doi:10.1088/0953-8984/21/11/115402

Probing hydrogen interactions with amorphous metals using first-principles calculations

Shiqiang Hao[1,2], M Widom[3] and David S Sholl[4,5]

[1] Department of Chemical Engineering, Carnegie Mellon University, Pittsburgh, PA 15213, USA
[2] National Energy Technology Laboratory, Pittsburgh, PA 15236, USA
[3] Department of Physics, Carnegie Mellon University, Pittsburgh, PA 15213, USA
[4] School of Chemical and Biomolecular Engineering, Georgia Institute of Technology, Atlanta, GA 30332-0100, USA

E-mail: david.sholl@chbe.gatech.edu

Received 10 November 2008, in final form 29 January 2009
Published 19 February 2009
Online at stacks.iop.org/JPhysCM/21/115402

Abstract

Amorphous metals are interesting candidates for use as H_2 purification membranes and occur in some applications of H_2 storage. We introduce a general strategy combining density functional theory and statistical mechanics for quantitatively predicting the properties of interstitial H in amorphous metals. We systematically investigate H solubility in amorphous Fe_3B, comparing our results with ones for a crystalline material with the same composition. H–H interactions in the amorphous material play a crucial role in determining the net solubility. H solubility in the amorphous and crystalline materials differs by orders of magnitude under conditions relevant for practical H_2 purification membranes. Our results give atomic-level insight into the properties of H in amorphous metals that has not been previously available.

(Some figures in this article are in colour only in the electronic version)

1. Introduction

Dramatic differences exist between the properties of amorphous and crystalline metal alloys. It is not surprising, therefore, that large differences exist between the behavior of interstitial H in amorphous and crystalline metals. Two recent reviews identified amorphous metal films as one of the most promising avenues for the development of robust H_2 purification membranes [1, 2]. Amorphous light metal hydrides have also been reported in materials of significant interest for reversible H_2 storage [3]. In both of these applications, understanding the equilibrium solubility of H in the material as a function of temperature and the external pressure of H_2 is a prerequisite for considering the suitability of a material for practical applications.

In studies of crystalline hydrides, density functional theory (DFT) has become a valuable complement to experimental approaches [4–8]. In contrast, previous theoretical models of H in amorphous metals have been phenomenological [1, 2, 9–11]. These models give useful qualitative information, but they cannot make quantitative predictions with the aim of discovering new materials for specific applications. This situation means that it is not currently possible to assess the potential use of amorphous materials in applications aiming to purify or store H_2.

In this paper, we show how DFT calculations can be used to quantitatively describe interstitial H in amorphous metals. Although numerous studies have used DFT to probe the structure of amorphous materials in the past [12–15], several novel challenges had to be overcome to extend the application of these calculations to describe interstitial H. First, we introduce methods that can systematically identify the large number of different interstitial sites that can exist in amorphous metals without requiring assumptions to be made about the geometric characteristics of these sites. We then show how DFT calculations can be used to assess the interactions that exist between nearby interstitial H atoms in an amorphous material. These interactions are found to

[5] Author to whom any correspondence should be addressed.

play a large role in determining the overall solubility of H, and our DFT results allow their effects to be described in a quantitative way. With this information from DFT calculations, it is possible to efficiently describe the solubility of H as a function of H_2 pressure and temperature using grand canonical Monte Carlo simulations. A brief account of some of our results has already appeared [16], but this paper presents a more detailed description of our calculations that expands on several important issues that were touched upon in brief terms in our previous report. In this paper, we introduce these methods by examining a specific amorphous material, Fe_3B, and comparing the properties of this material with a crystalline material with the same stoichiometry. A useful feature of our methods, however, is that they will be applicable to any amorphous metal, so these methods should be useful in considering the performance of these materials in a range of applications.

2. Calculation details

Throughout the paper, we focus on the solubility of H in amorphous Fe_3B (a-Fe_3B). From previous DFT studies of glass formation in Fe-based alloys, it is known that a crystalline analogue of a material with the same stoichiometry exists with a slightly larger cohesive energy than the amorphous phase [17]. This crystalline material has Pearson symbol oP16, and we denote it below by c-Fe_3B. Comparing these two stoichiometrically identical structures is a useful way to highlight the differences that exist in the solubility of interstitial H in crystalline and amorphous materials.

All DFT calculations were performed with the Perdew–Wang 91 GGA functional [18] and projector augmented wave [19] potentials as implemented in VASP [20]. Spin polarization with Vosko–Wilk–Nusair spin interpolation [21] was used in all calculations. This significantly increases the computational effort associated with the calculations, but is required because of the magnetic properties of Fe. Calculations with the crystalline material used a supercell fixed in the DFT-optimized orthorhombic crystal structure with lattice parameters $a = 5.396$, $b = 6.636$ and $c = 8.758$ Å. This supercell contained 32 atoms, and our DFT calculations sampled k-space using $7 \times 5 \times 4$ k-points placed using the Monkhorst–Pack scheme. In energy minimizations, all atomic positions are relaxed until the forces exerted on each atom are less than 0.03 eV $Å^{-1}$.

To create a sample of amorphous Fe_3B suitable for use in DFT calculations, a supercell containing 100 atoms was created by applying *ab initio* molecular dynamics to a liquid like state at 1200 K, followed by a rapid temperature quench and then energy minimization [15]. The final supercell had lattice vectors $a = 9.159$, $b = 10.145$ and $c = 10.058$ Å so the density of the amorphous material was 7.1% lower than the crystalline material. These calculations sampled k-space at the Γ-point only. A test calculation using $2 \times 2 \times 2$ k-points gave an interstitial H binding energy that differed from the value calculated sampling k-space at the Γ-point by ∼0.01 eV. The reliability of the resulting amorphous structure can be assessed by comparison with experimental structural data and also by comparison with prior simulations of similar materials. The partial pair distribution functions, $G_{\alpha\beta}$, resemble those found experimentally for a-$Fe_{75}B_{25}$ and a-$Fe_{80}B_{20}$ [22, 23] and also those obtained by prior first-principles replica exchange simulations of $Fe_{80}B_{20}$ [15]. Key points of agreement include strong first peaks at 2.2 Å and 2.6 Å in G_{FeB} and G_{FeFe} respectively, and split second peaks at 3.9–4.6 Å and 4.1–5.0 Å, respectively. G_{BB} was not determined experimentally for a-$Fe_{75}B_{25}$, but our second peak at 3.4 Å agrees well with the experimental structure of a-$Fe_{80}B_{20}$. We also observe a weak first peak in G_{BB} at 1.9 Å corresponding to B–B bonding that is not seen experimentally in the G_{BB} partial structure factor at the lower B concentration [23], although it might be present at the higher B concentration [24].

At a more local level, we can examine individual simulated atomic environments. Although these cannot be directly compared with experimental results, we can compare our $Fe_{75}B_{25}$ structure with the ensemble of $Fe_{80}B_{20}$ structures obtained by prior simulation [15]. The most numerous boron environment is the 'trigonal prism' of Voronoi type (0, 3, 6), followed by a distorted trigonal prism of type (0, 5, 4) and the Kasper polyhedron of Voronoi type (0, 2, 8). Together, these account for about half of all boron environments, the same as was found in the prior simulation. Among iron environments, we find a variety of icosahedra of Voronoi type (0, 0, 12), distorted icosahedra and higher Kasper polyhedra [13, 15], with a distribution again similar to that found for $Fe_{80}B_{20}$. Based on these comparisons, we conclude that the specific 100-atom sample amorphous structure used in the present study is typical of the ensemble of amorphous structures that exist for this composition and that it shares local order out to at least 5 Å with the true amorphous material.

Test calculations showed that placing individual H atoms in the supercells defined by either a-Fe_3B or c-Fe_3B caused only small changes in their lattice constants (<0.2% and <1.5% for a-Fe_3B and c-Fe_3B, respectively). As a result all calculations reported below fixed the supercell size and volume to be that of the structurally optimized H-free materials. In energy minimizations involving interstitial H, all atomic positions (not just the H atom or atoms) were relaxed. Zero point energies were computed in the harmonic approximation, and for interstitial H we assumed that H vibrations were decoupled from lattice phonons.

3. Binding sites for individual H atoms

In crystalline materials, locating potential interstitial sites for H is typically straightforward based on symmetry considerations. In amorphous materials, however, this task is more challenging. To avoid introducing bias, it is important that methods be developed to locate all interstitial sites without making assumptions about the structure of these sites. We approached this task in two stages. First, we used empirical pair potentials for H–Fe and H–B interactions to define the energy of individual H atoms with the positions of all Fe and B atoms fixed. We used Fe–Fe, B–B and H–H potentials from previous work [25–27], and applied the Lorentz–Berthelot mixing rules to define H–Fe and H–B interactions. Using

these potentials, the energy of H atoms was minimized from all points defining a grid with resolution 0.02 nm × 0.02 nm × 0.02 nm in each supercell. Any minimum identified by these calculations that was located more than 0.9 Å from other previously identified minima was considered to be a distinct minimum within the structure. This procedure identified 196 candidate energy minima in the supercell for a-Fe_3B.

The second stage in our calculations was to use each of the candidate energy minima identified as defined above as initial structures in DFT energy minimizations. In these DFT calculations, all atoms in the supercell were allowed to relax. This procedure was applied to both the crystalline and the amorphous supercells. In a small number of cases, two or more candidate minima generated from the empirical potential described above converged to a single minimum when relaxed with DFT. These DFT calculations identified 4 structurally distinct interstitial sites in c-Fe_3B and 174 sites in a-Fe_3B. It is useful to note that this two step approach to locating the positions of interstitial H in complex materials could readily be adapted to amorphous metals of any composition.

Once all the interstitial sites for H in each material were found, the binding energy of H in each site was defined by [4]

$$E_b = E_{host/H} - E_{host} - \tfrac{1}{2}E_{H_2} + E^{ZP}_{host/H} - \tfrac{1}{2}E^{ZP}_{H_2}, \quad (1)$$

where E_{host} ($E_{host/H}$) is the energy of the system without (with) atomic H in the host lattice, E_{H_2} is the energy of a free H_2 molecule, and $E^{ZP}_{host/H}$ ($E^{ZP}_{H_2}$) is the zero point energy contribution from H in the host lattice (in a free molecule).

Figure 1 shows the binding energies for all interstitial sites in a-Fe_3B and c-Fe_3B. For ease of visualization, each of the 174 discrete binding energies in a-Fe_3B was plotted using a Gaussian with width 0.015 eV. In the crystalline material, H in the octahedral Fe_6 sites has $E_b \approx 0$, while the three tetrahedral sites (two distinct Fe_4 sites and one Fe_3B site) are considerably less favorable.

The amorphous material shows the characteristics that have been identified in previous experimental studies of amorphous alloys [3, 9, 28]. In particular, a broad range of binding energies is observed, including a large number of sites that bind H much more favorably than the crystalline material. The most favorable binding sites in the amorphous material have binding energies more than 0.5 eV lower than the octahedral Fe_6 sites in crystalline Fe_3B. This energy difference is large compared to the range of binding energies that are typically observed due to alloying effects in crystalline interstitial metal hydrides [4, 29]. Almost half of all the interstitial sites in the amorphous material have binding energies that are more favorable than the octahedral Fe_6 sites in crystalline Fe_3B.

The majority of the interstitial sites in a-Fe_3B are distorted versions of the crystalline material's Fe_6 and Fe_4 sites. We determined the fraction of sites of each kind in a-Fe_3B as a function of energy, where the site coordination was defined by counting all atoms within 1.95 Å of the H atom. This distance unambiguously defines the site types in the crystalline material. Using this definition, 21.9/33.7/37.1% of the sites in the amorphous material with $E_b \leqslant 0$ are Fe_6/Fe_5/Fe_4 sites. The remaining 7.4% of sites in this energy range includes Fe_3B, Fe_3B_2, and Fe_4B_1. If all atoms within 2.30 Å of the H atom are counted, then 48.9% of the sites with $E_b \leqslant 0$ are Fe_6 sites.

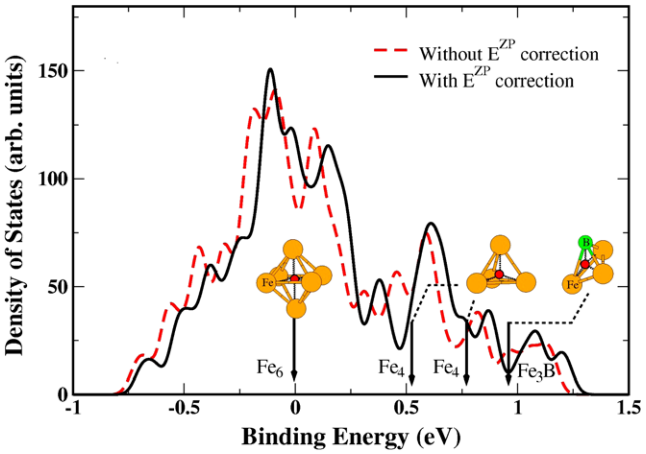

Figure 1. H binding energy distribution in a-Fe_3B. The arrows indicate the zero point corrected H binding energy in a site in c-Fe_3B.

Figure 1 also shows the effect of including zero point corrections in the binding energies of interstitial H in a-Fe_3B. These effects make slight differences in the energies of the individual binding sites, but the distribution of binding site energies is not qualitatively changed by neglecting zero point corrections. The zero point energies of interstitial H can be related to the vibrational density of states (VDOS) that has been measured for a number of amorphous materials (although not for Fe_3B) using neutron spectroscopy [30]. The calculated VDOS for crystalline and amorphous Fe_3B are consistent with the qualitative trends seen experimentally; the VDOS in the amorphous material covers a broader range of energies than the crystalline material. In crystalline materials, it is reasonable to expect that the most favorable binding sites will have lower vibrational frequencies for H than sites that are less energetically favorable, and this expectation is borne out in a number of examples where it has been tested [31]. This heuristic description is correct for c-Fe_3B in the sense that we find that the most favored site does have the lowest zero point energy among all sites in this material. Our results show, however, that this description is not valid for amorphous materials. Instead, our data for a-Fe_3B shows no clear correlation between E_b and the vibrational frequencies of interstitial H [16].

4. H–H interactions

When the binding energies of interstitial H atoms in a material are unfavorable with respect to gaseous H_2 (or are only marginally favorable), the solubility of H in this material will be low, even under relatively high pressures of H_2. This situation occurs in many of the crystalline metals that are used as membranes for H_2 purification, and it means that these membrane materials can be analyzed in terms of individual interstitial H atoms [1, 4, 32]. It is clear from the binding energies shown in figure 1 that c-Fe_3B can also be described

in this way. When individual binding sites exist with binding energies that are highly favorable relative to gaseous H_2, however, appreciable concentrations of interstitial H will exist even for moderate pressures of H_2. In this situation, it is important to understand whether interactions among interstitial atoms in the material will play a role in the material's net solubility.

To probe the effects of H–H interactions in a-Fe_3B, we used DFT to compute the interaction energy of a large number of H–H pairs with the H atoms located in nearby interstitial sites. In these calculations, the two H atoms were placed in the positions determined to be energy minima for the individual interstitial sites, then all atoms in the supercell were allowed to relax during energy minimization. After relaxation, the interaction energy for a pair of H atoms was defined by

$$\Delta E_{\mathrm{H-H}} = E_{\mathrm{host/2H}} + E_{\mathrm{host}} - E_{\mathrm{host/H,1}} - E_{\mathrm{host/H,2}}. \qquad (2)$$

Here, $E_{\mathrm{host/2H}}$ is the energy of the supercell including both H atoms and $E_{\mathrm{host/H,1}}$ ($E_{\mathrm{host/H,2}}$) is the energy of the optimized supercell containing only the first (second) H atom. Zero point energies were not included in this analysis. With this definition, values of $\Delta E_{\mathrm{H-H}} > 0$ correspond to repulsive H–H interactions. Calculations were performed for 35 distinct pairs, some in which the individual binding energies of one or both interstitial sites (including zero point energies) was <-0.2 eV, and some for which both individual sites were less energetically favored. Although attractive interaction energies are known for some crystalline metals [33] and dense metal sulfides [34], we did not observe any site pairs with $\Delta E_{\mathrm{H-H}} < 0$ in a-Fe_3B. The calculated $\Delta E_{\mathrm{H-H}}$ are summarized in figure 2, where the H–H distance is characterized using the distance between H atoms prior to relaxation of the H–H pair. The data in figure 2 shown with open squares comes from site pairs where one or both individual site binding energies was <-0.2 eV. There is no obvious difference in the interaction energies between these favorable site pairs and the other site pairs we examined. Our DFT results are empirically described with reasonable accuracy with a simple exponential function, as shown by the solid curve in figure 2.

H–H interactions in metals are often characterized via the Westlake criterion, an empirical prediction that two nearby interstitial sites cannot be simultaneously occupied by H atoms if the distance between the sites is less than 0.21 nm [35]. The results in figure 2 create an interesting opportunity to consider the precision of this criterion. Our results are reasonably consistent with the Westlake criterion if the distribution of a fixed number of H atoms in the host is considered, since in this case the energy penalty for placing H atoms in two sites that are closer than 0.21 nm is 0.2 eV or more. A discussion of whether 0.2 eV represents a 'large' repulsive interaction depends on the temperature of interest. A more subtle situation arises if the occupation of sites in an open system that is in equilibrium with an external H_2 reservoir is considered, as is necessary to examine the equilibrium solubility of H. We found that pairs of sites exist that could not both be occupied according to the Westlake criterion which nevertheless both have negative binding energies relative to gaseous H_2 even after including the repulsive H–H interactions. This occurs because of the very favorable binding energies of the individual interstitial sites relative to gaseous H_2.

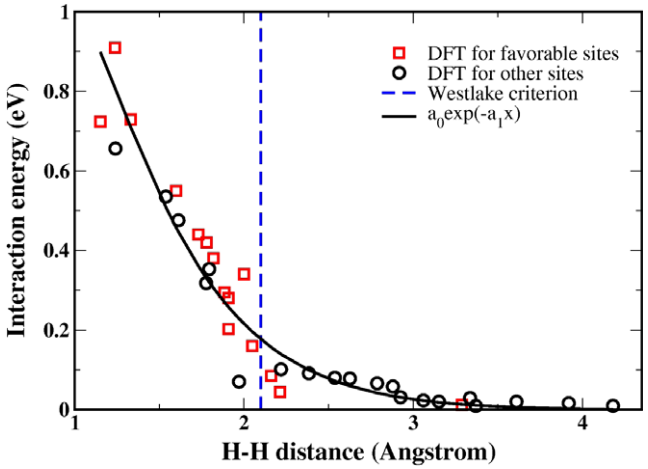

Figure 2. Calculated H–H interaction energies for 35 distinct H–H pairs in a-Fe_3B. The parameters for the fitted solid line are $a_0 = 5.68$ eV and $a_1 = 1.61$ Å^{-1}.

5. H solubility in amorphous and crystalline Fe_3B

We used the results above to predict the solubility of H in a-Fe_3B and c-Fe_3B. Once the site energies and H–H interaction energies were defined, H solubility was calculated using grand canonical Monte Carlo calculations that treated H_2 as an ideal gas [36]. This method agreed with a more direct statistical mechanics calculation that is valid in the limit of low H concentrations [4]. The dashed curves in figures 3(a) and (b) show the calculated H solubility at 400 and 600 K from calculations that used the site energies obtained from DFT (i.e. the density of states shown in figure 1) and treated H–H interactions using the exponential curve shown in figure 2. Here and below, solubility is characterized using the ratio of H atoms to host atoms, H/M. When $p = 1$ atm, $H/M = 0.114$ (0.055) at 400 (600) K. Because of the broad distribution of site binding energies, the solubility does not vary strongly with the H_2 pressure; reducing the H_2 pressure to 10^{-4} atm only reduces H/M to 0.061 (0.012) at 400 K (600 K). These results represent the first time that it has been possible to make quantitative predictions of H solubility in an amorphous metal.

The results in figure 3 are useful for exploring the phenomena that control the solubility of H in this amorphous material. To describe this issue, figure 3 shows data from several approximate treatments of H solubility in a-Fe_3B. First, H solubility was calculated using the site energies calculated from DFT but neglecting H–H interactions. The results from this simple approximation are shown as open circles in figure 3. This approach strongly overestimates the H solubility, highlighting the crucial role of H–H interactions in determining the true solubility of H in materials of this kind.

A more refined approach to describing H solubility that does not require detailed information on H–H interactions is to approximate these interactions as a hard wall potential via the Westlake criterion. With this approach, the formation

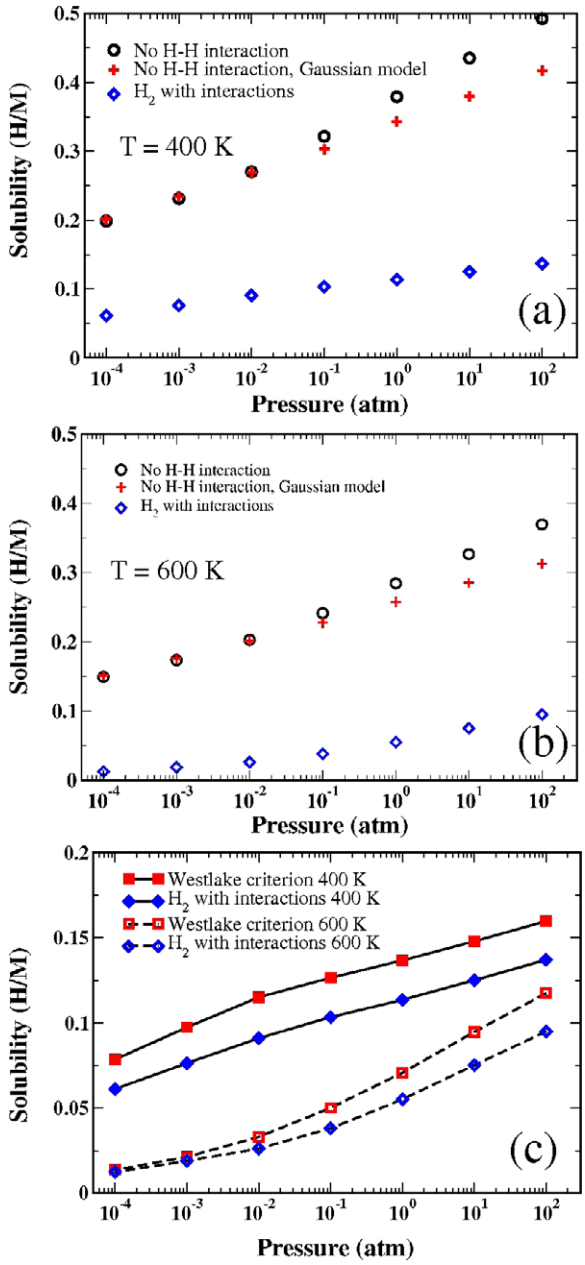

Figure 3. The predicted solubility of H in a-Fe_3B as a function of H_2 pressure at (a) 400 K, (b) 600 K, and (c) comparison with Westlake criterion. The symbols in (a) and (b) show results for several approximate treatments of H_2 as explained in the text.

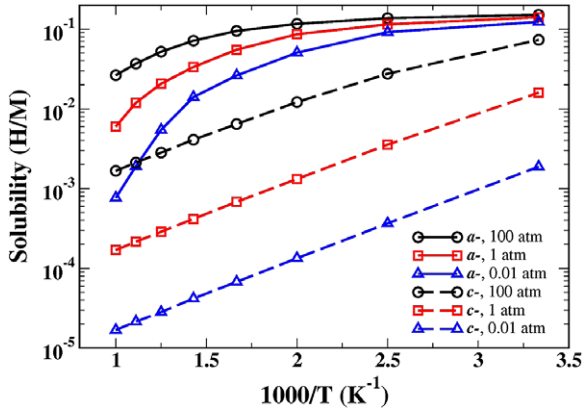

Figure 4. Calculated H solubility in a-Fe_3B (solid curves) and c-Fe_3B (dashed curves) as a function of temperature and H_2 pressure. Lines are guides to the eye.

of H–H pairs with H–H distances <0.21 nm (characterized via the positions of the individual interstitial site minima) are excluded during our GCMC simulations. Results from this approach at 400 and 600 K are shown in figure 3(c). This simple model of interactions strongly reduces the H solubility relative to the approximation with no H–H interactions, and gives results in qualitative agreement with the more detailed approach of describing H–H interactions used above. Using the Westlake criterion in this way overestimates the H solubility because it neglects the repulsive interactions that exist for H–H atoms with distances >0.21 nm. At $p = 1$ atm, 400 K, the approximate treatment based on the Westlake criterion gives a solubility 9% larger than our detailed calculation. At higher temperatures and low pressures, in contrast, the solubility predicted by this simplified model is in better agreement with our detailed calculations because H–H interactions play a weaker role under these conditions.

Phenomenological models of H in amorphous materials have often described site energies using a Gaussian distribution [9, 10, 28, 37] or sums of Gaussian distributions [38]. To explore how valid a model of this kind can be for describing solubility, we approximated our calculated DOS in figure 1 using a single Gaussian with the same mean (+0.081 eV) and standard deviation (0.427 eV) as our full set of interstitial sites. The solubility predicted by this distribution (neglecting H–H interactions) is shown in figure 3. The qualitative agreement with calculations based on the full energy DOS is good, but quantitative differences between the calculations exist. The simple Gaussian model cannot be quantitatively accurate in the limit of low H/M, since this limit is dominated by a small number of the most favorable sites and these sites do not make a large contribution to the mean and standard deviation of the overall DOS. It is important to note that it would not be possible to combine a model based on one or a sum of Gaussian distribution of site energies with a description of H–H interactions via the Westlake criteria (or a related approximation) without imposing a model for the spacing for all interstitial sites. In our detailed calculations, this complication does not arise because we have identified the location of each interstitial site prior to determining the site binding energies.

The solubility of H in a-Fe_3B and c-Fe_3B as a function of temperature and pressure is contrasted in figure 4. The solubility of H in c-Fe_3B follows a simple Arrhenius form because this solubility is dominated by a single kind of interstitial site. This solubility also follows a simple Sieverts' law dependence on pressure, so increasing the H_2 pressure by two orders of magnitude increases the solubility of interstitial H by one order of magnitude. The solubility of H in the amorphous material is more complicated because of the nontrivial distribution of site energies that are present in this material and the effects of H–H interactions. As

the temperature is reduced, the solubility of H in the amorphous material tends towards saturation as the lowest energy interstitial sites are fully occupied. At the highest pressure shown in figure 4, the H content of a-Fe_3B is approximately one order of magnitude larger than c-Fe_3B. At lower pressures, the differences between the materials are more dramatic. At 600 K, for example, the ratio of H in a-Fe_3B to c-Fe_3B is ∼500 when $p = 0.01$ atm.

6. Solubility of H isotopes in amorphous and crystalline Fe_3B

Because our calculations provide detailed information on the vibrational frequencies of interstitial H in each site, we can use our data to examine the differences that exist between crystalline and amorphous metals for isotopic separations. In low temperature applications, hydrogen isotope separations can be achieved using adsorption in porous materials or in metals [39, 40]. Membranes based on dense metal films raise interesting opportunities for achieving isotopic separations at high temperatures [39, 41–44].

To explore whether amorphous metals might have some advantages over crystalline materials for isotopic separations, we examined the solubility of D_2 and T_2 in c- and a-Fe_3B. We calculated the solubility of each isotope using the site energies and zero point energies defined above, treating all zero point energies within the harmonic approximation. Our results are shown in figure 5. Qualitatively, our results agree with the experimental observation in pure Pd that solubility increases in the order T < D < H [45]. Similar to pure Pd, the relative solubility of the isotopes in c-Fe_3B increasingly favors the lighter isotopes as the temperature is reduced.

The characteristics of isotopic adsorption in the amorphous and crystalline materials are quite different. At all temperatures, the relative solubility of the lighter isotopes is less dramatic in the amorphous material than in c-Fe_3B. At the lowest temperatures shown in figure 5, there is essentially no isotopic selectivity in the amorphous material. This situation is due to the very favorable binding energies found in some interstitial sites in this material. These values create strong trap sites regardless of the isotope, and these trap sites dominate the overall solubility of the material. At the highest temperatures we examined, the occupancy in these strong trap sites decreases and the difference in the ZPE amongst the isotopes has a stronger effect on the solubility.

7. Conclusion

We have introduced a strategy for quantitatively predicting H solubility in amorphous metals using DFT calculations. Our approach provides insights that were not accessible via previous experiments or phenomenological theories. Because these methods could be applied to any amorphous alloy, they should find uses in screening materials for practical applications. As was already known from phenomenological descriptions of H in amorphous metals, the broad range of interstitial site energies in amorphous materials leads to a variety of behaviors that differ dramatically from crystalline

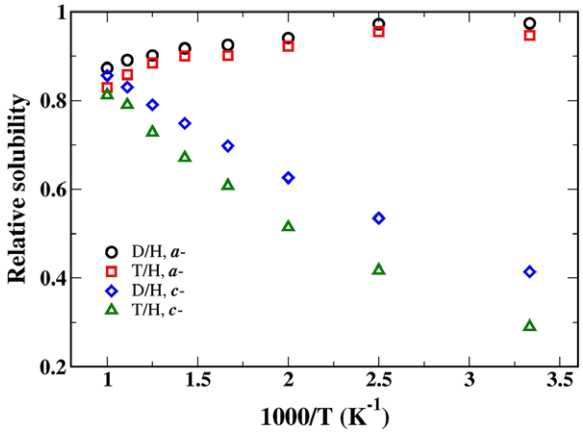

Figure 5. Solubility of deuterium (D) and tritium (T) relative to H in a-Fe_3B and c-Fe_3B as a function of temperature at 1 atm.

materials. One consequence of the broad site energy distribution is that the solubility of H in an amorphous material is typically far larger than in analogous crystalline materials. Our calculations make it possible to make quantitative predictions about the size of this effect. We showed one example where the difference in solubility between a crystalline and an amorphous material was a factor of 500 under relatively mild conditions.

A second consequence of the site energy distribution in amorphous materials is that interactions between interstitial H atoms play a crucial role in determining the net solubility of H. Our results showed that using the Westlake criterion can describe the repulsive interactions that exist between nearby interstitial H atoms, but that using this criterion alone is not sufficient if quantitative predictions are desired over a broad range of conditions. Our DFT calculations indicate that repulsive H–H interactions in amorphous Fe_3B can be described in a satisfactory way with a simple exponential function that can then be used in detailed GCMC simulations of H solubility.

We also examined the solubility of hydrogen isotopes in crystalline and amorphous Fe_3B. The main observation from these calculations is that the amorphous material shows little isotopic selectivity. This outcome is a direct consequence of the high solubility of H in this material; the amorphous material includes a large number of interstitial sites that are occupied with high probability even under mild conditions, so there is limited scope for the net solubility of H in the material to be isotopically selective. Our calculations involving isotopes are limited in the sense that they only consider a material in equilibrium with pure H_2, D_2, or T_2. If a complete treatment of isotopic separations was desirable, the solubility and gas phase equilibrium between appropriate mixtures of these species and the mixed isotope molecules, HD, HT, and DT, would be necessary.

It is important to note that our calculations make no predictions about the temperatures at which recrystallization would change amorphous Fe_3B into its crystalline form. Examples are known for crystalline metal alloys where the presence of interstitial H can induce lattice rearrangements [46–49]. It is conceivable that interstitial H could play

a similar role in the recrystallization of amorphous alloys, acting to either depress or raise the temperature at which recrystallization can occur. It is well beyond the scope of our calculations, however, to make predictions about this phenomenon.

Acknowledgments

SH and DSS were supported by funds from the US DOE Hydrogen Fuels Initiative. MW was supported by the DARPA Structural Amorphous Metals Program under ONR Grant No. N00014-06-1-0492.

References

[1] Ockwig N W and Nenoff T M 2007 *Chem. Rev.* **107** 4078–110
[2] Dolan M D, Dave N C, Ilyushechkin A Y, Morpeth L D and McLennan K G 2006 *J. Membr. Sci.* **285** 30–55
[3] Wu H, Zhou W, Udovic T J and Rush J J 2007 *Chem. Mater.* **19** 329–34
[4] Kamakoti P, Morreale B D, Ciocco M V, Howard B H, Killmeyer R P, Cugini A V and Sholl D S 2005 *Science* **307** 569–73
[5] Kamakoti P and Sholl D S 2006 *J. Membr. Sci.* **279** 94
[6] Alapati S V, Johnson J K and Sholl D S 2006 *J. Phys. Chem.* B **110** 8769
[7] Alapati S V, Johnson J K and Sholl D S 2007 *Phys. Chem. Chem. Phys.* **9** 1438
[8] Akbarzadeh A R, Ozolins V and Wolverton C 2007 *Adv. Mater.* **19** 3233
[9] Kirchheim R, Mutschele T, Kieninger W, Gleiter H, Birringer R and Koble T D 1988 *Mater. Sci. Eng.* **99** 457–62
[10] Kirchheim R 2001 *Phys. Scr.* **94** 58–67
[11] Brouwer R C and Griessen R 1989 *Phys. Rev.* B **40** 1481–94
[12] Jakse N and Pasturel A 2003 *Phys. Rev. Lett.* **91** 1995501
[13] Sheng H W, Luo W K, Alamgir F M, Bai J M and Ma E 2006 *Nature* **439** 419–25
[14] Sheng H W, Liu H Z, Cheng Y Q, Wen J, Lee P L, Luo W K, Shastri S D and Ma E 2007 *Nat. Mater.* **6** 192–7
[15] Ganesh P and Widom M 2008 *Phys. Rev.* B **77** 014205
[16] Hao S and Sholl D S 2008 *Energy Environ. Sci.* **1** 175–83
[17] Mihalkovič M and Widom M 2004 *Phys. Rev.* B **70** 144107
[18] Perdew J P and Wang Y 1992 *Phys. Rev.* B **45** 13244
[19] Kresse G and Joubert D 1999 *Phys. Rev.* B **59** 1758
[20] Kresse G and Furthmuller J 1996 *Comput. Mater. Sci.* **6** 15–50
[21] Vosko S H, Wilk L and Nusair M 1980 *Can. J. Phys.* **58** 1200
[22] Matz W, Hermann H and Mattern N 1987 *J. Non-Cryst. Solids* **93** 217–29
[23] Nold E, Lamparter P, Olbrich H, Rainerharbach G and Steeb S 1981 *Z. Naturf.* a **36** 1032–44
[24] Hoving W, Egami T, Vincze I and Vanderwoude F 1987 *J. Physique* E **20** 188–92
[25] Mohri T, Horiuchi T, Uzawa H, Ibaragi M, Igarashi M and Abe F 2001 *J. Alloys Compounds* **317/318** 13–8
[26] Thamwattana N and Hill J M 2007 *J. Phys.: Condens. Matter* **19** 406209
[27] Kowalczyk P, Tanaka H, Holyst R, Kaneko K, Ohmori T and Miyamoto J 2005 *J. Phys. Chem.* B **109** 17174–83
[28] Kirchheim R 1988 *Prog. Mater. Sci.* **32** 261–325
[29] Semidey-Flecha L and Sholl D S 2008 *J. Chem. Phys.* **128** 144701
[30] Rush J J, Rowe J M and Maeland A J 1980 *J. Phys. F: Met. Phys.* **10** L283–5
[31] Kamakoti P and Sholl D S 2003 *J. Membr. Sci.* **225** 145
[32] Kamakoti P and Sholl D S 2005 *Phys. Rev.* B **71** 014301
[33] Sholl D S 2007 *J. Alloys Compounds* **446** 462
[34] Ling C and Sholl D S 2008 *J. Membr. Sci.* at press
[35] Westlake D G 1983 *J. Less-Common Met.* **91** 1–20
[36] Ling C and Sholl D S 2007 *J. Membr. Sci.* **303** 162
[37] dos Santos D S and Miranda P E V 1997 *J. Mater. Sci.* **32** 6311
[38] Bankmann J, Pundt A and Kirchheim R 2003 *J. Alloys Compounds* **356/357** 566–9
[39] Aoki K, Ogata Y, Kasakabe K and Morooka S 1998 *Int. J. Hydrog. Energy* **23** 325–32
[40] Wang Q, Challa S, Sholl D S and Johnson K J 1999 *Phys. Rev. Lett.* **82** 956
[41] Evans J and Harris I R 1983 *J. Less-Common Met.* **89** 407–14
[42] Dudek D 2007 *J. Alloys Compounds* **442** 152
[43] Matsuyama M, Sugiyama H, Hara M and Watanabe K 2007 *J. Nucl. Mater.* **367–370** 1096–101
[44] Serra E, Kemali A, Perujo A and Ross D K 1998 *Metall. Mater. Trans.* A **29** 1023–8
[45] Lässer R 1984 *Phys. Rev.* B **29** 4765–8
[46] Noh H 1996 *J. Alloys Compounds* **240** 235
[47] Park C N 1997 *Scr. Mater.* **37** 1709
[48] Flanagan T B 1999 *J. Alloys Compounds* **293** 161
[49] Lee S-M, Noh H, Flanagan T B and Luo S 2007 *J. Phys.: Condens. Matter* **19** 326222